

Wahlfachpraktikum in der Arbeitsgruppe Elektronenmikroskopie:

TEM & EELS¹

Transmission Electron Microscopy
and
Electron Energy Loss Spectroscopy



Quelle:

B. Fultz and J. M. Howe: Transmission Electron Microscopy and Diffractometry of Materials, Springer 2008 (3. Aufl.)

Online-Zugriff:

<http://dx.doi.org/10.1007/978-3-540-73886-2>

¹Stand: 27. März 2015

Inhalt der Anleitung

Die Anleitung enthält keine Beschreibungen der Versuche, sondern es werden die theoretischen Grundlagen zum Verständnis der durchgeführten Versuche vermittelt. Ähnlich zu den Experimentelle Übungen 2 wird dabei auf vorhandene Literatur zurückgegriffen. Die folgenden Themen werden behandelt:

- 2. The TEM and its Optics (S. 61 - 63)
 - 2.1 Introduction to the Transmission Electron Microscope (S. 61 - 63)
- 4. Inelastic Electron Scattering and Spectroscopy (S. 163)
 - 4.1 Inelastic Electron Scattering (S. 163 - 165)
 - 4.2 Electron Energy-Loss Spectrometry (EELS). (S. 165 - 168)
 - 4.2.1 Instrumentation
 - 4.2.2 General Features of EELS Spectra
 - 4.3 Plasmon Excitations (S. 173 - 177)
 - 4.3.1 Plasmon Principles
 - 4.3.2 * Plasmons and Specimen Thickness
 - 4.4 Core Excitations (S. 191 - 193)
 - 4.4.7 Quantification of EELS Core Edges
 - 4.5 Energy-Filtered TEM Imaging (EFTEM) (S. 193 - 199)
 - 4.5.1 Spectrum Imaging
 - 4.5.2 Energy Filters
 - 4.5.3 Chemical Mapping with Energy-Filtered Images
 - 4.5.4 Chemical Analysis with High Spatial Resolution

Die angegebenen Seitenzahlen beziehen sich auf das Buch **Transmission Electron Microscopy and Diffractometry of Materials** von Brent Fultz und James M. Howe in der dritten Auflage von 2008. Die URL zum Buch (Springerlink) ist auf der Titelseite zu finden.

Möglicher Ablauf des Versuch TEM & EELS

Bei diesem Versuch geht es darum die Methode Electron Energy Loss Spectroscopy (EELS) kennen zu lernen. Gearbeitet wird an einem modernen Transmissionselektronenmikroskop der Firma Carl Zeiss, dem Zeiss Libra 200FE. Dabei handelt es sich um ein Gerät, das mit einer Beschleunigungsspannung von 200kV arbeitet und abbildenden Energiefilter besitzt.

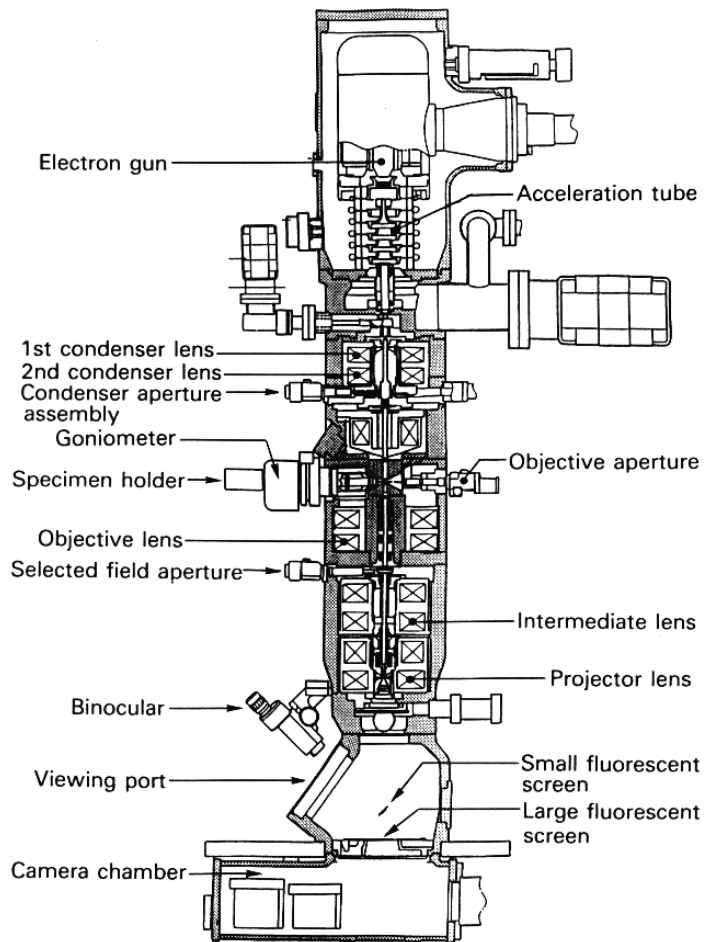
Bei der Auswahl der Probe(n) kann auf die Wünsche der Teilnehmer eingegangen werden. Etabliert hat sich aber ein Eisen-Chrom Schichtsystem auf einem Silizium-Wafer. Sämtliche Methoden lassen sich gut an dieser Probe zeigen, wobei neben den Vorteilen der einzelnen Methoden auch deren Nachteile gezeigt werden können. Im Folgenden wird ein möglicher Ablauf des Versuch aufgezeigt.

- Bestimmung der Probendicke (relativ und absolut) mit einem Low-Loss Spektrum.
- Bestimmung der ortsabhängigen, relativen Probendicke durch gefilterte und ungefilterte Bilder.
- Untersuchung von Plasmonpeaks und M-Kanten (Fe & Cr).
- Auswirkungen unterschiedlicher Probendicken (Mehrfachstreuung).
- Quantifizierung von Eisen und Chrom mit Hilfe der L-Kanten.
- Durchführung von Spectrum Imaging im Low-Loss Bereich.
- Korrektur und kurze Auswertung des Spectrum Imaging Datensatzes.
- Aufnahme von gefilterten Bildern und deren Auswertung. Das Ziel ist es Elementverteilungsbilder zu erstellen, welches mehrere Elemente gleichzeitig zeigt.

Protokoll

Wir erwarten kein vollständiges Protokoll von euch, so wie es bisher bei den experimentellen Übungen üblich war. Statt dessen reicht ein kurzer Bericht aus. Das bedeutet, dass ihr nicht detailliert auf die theoretischen Grundlagen eingehen sollt. Beim Schreiben des Protokolls könnt ihr davon ausgehen, dass auch der Leser die euch zur Verfügung stehende Literatur kennt und ihr müsst sie deshalb nicht nochmal in eigenen Worten wiedergeben. Die Beschreibung der Versuchsdurchführung und eine kurze Erläuterung der erzielten Ergebnissen ist ausreichend.

2. The TEM and its Optics



2.1 Introduction to the Transmission Electron Microscope

The transmission electron microscope (TEM) has become the premier tool for the microstructural characterization of materials. In practice, the diffraction patterns measured by x-ray methods are more quantitative than electron diffraction patterns, but electrons have an important advantage over x-rays;

electrons can be focused easily. By focusing the electron beam, diffraction patterns as discussed in Chapter 1 can be measured from microscopic regions, and it is often possible to select a single microcrystal for a diffraction measurement. The optics of electron microscopes can be used to make images of the electron intensity emerging from the sample. For example, variations in the intensity of electron diffraction across a thin specimen, called “diffraction contrast,” is useful for making images of defects such as dislocations, interfaces, and second phase particles. Beyond diffraction contrast microscopy, which measures the *intensity* of diffracted waves, in “high-resolution” transmission electron microscopy (HRTEM or HREM) the *phase* of the diffracted electron wave is preserved and interferes constructively or destructively with the phase of the transmitted wave. This technique of “phase-contrast imaging” is used to form images of columns of atoms. High-resolution images of atom columns are also possible with electron nanobeams incident on the sample, and electron scattering at high angles to minimize electron interference behavior (a method called “high-angle annular dark-field imaging”).

Besides diffraction and spatial imaging, the high-energy electrons in TEM cause electronic excitations of the atoms in the specimen. “Analytical TEM” uses two types of spectrometries to obtain chemical information from electronic excitations:

- In energy-dispersive x-ray spectrometry (EDS), an x-ray spectrum is acquired from small regions of the specimen illuminated with a focused electron beam, usually using a solid-state detector as described in Sect. 1.4.1. Characteristic x-rays from the chemical elements are used to determine the concentrations of the different elements in the specimen.
- In electron energy-loss spectrometry (EELS), energy losses of the electrons are measured after the high-energy electrons have traversed the specimen. Information on local chemistry and structure is obtained from features in EELS spectra caused by plasmon excitations and core electron excitations.

A block diagram of a TEM is shown in Fig. 2.1. A modern TEM may have the capability of imaging the variations in diffraction across the specimen (diffraction contrast imaging), imaging the phase contrast of the specimen (high-resolution imaging), obtaining diffraction patterns from selected areas of the specimen, and performing EELS and EDS spectroscopy measurements with a small, focused electron beam. A skilled microscopist can switch between these modes in seconds or minutes, allowing questions about the microstructure to be both posed and answered in short order during a session on the TEM.

In scanning transmission electron microscopy (STEM), a narrow (~ 1 – 10 \AA), focused beam of electrons is moved in a television-style raster pattern across the specimen. In synchronization with the raster scan, various data from the specimen are acquired, such as emitted x-rays, secondary electrons, or backscattered electrons. Transmitted electrons are detected with a moveable detector at the bottom of the microscope column. The STEM mode of

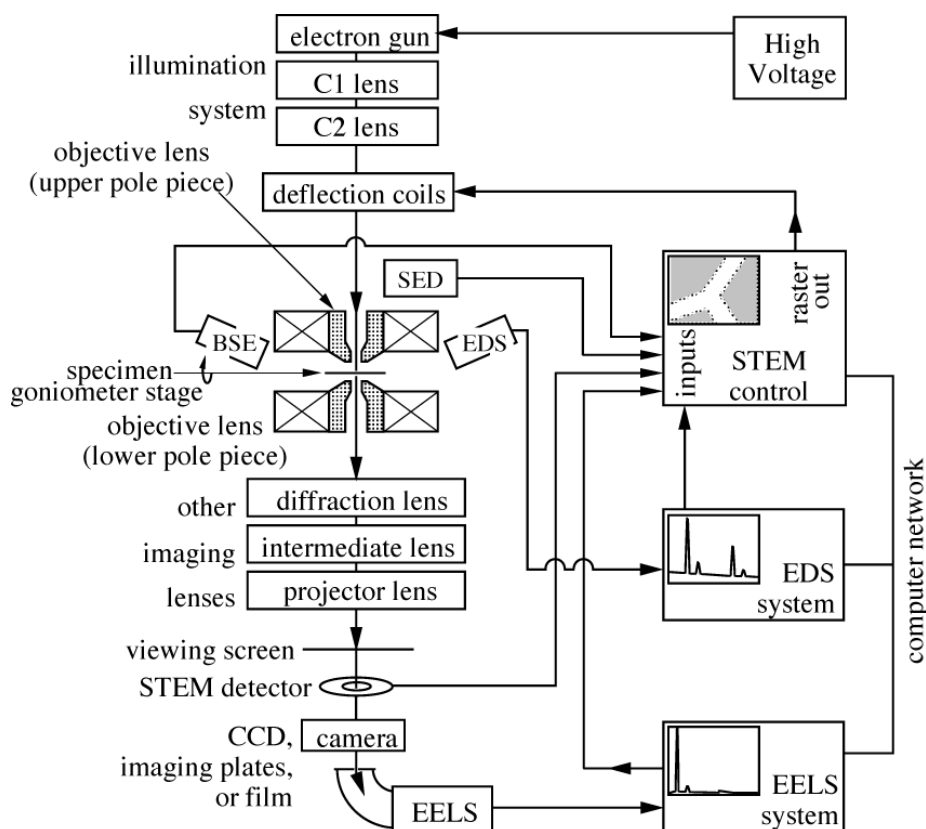


Fig. 2.1. Block diagram of typical TEM with STEM capability.

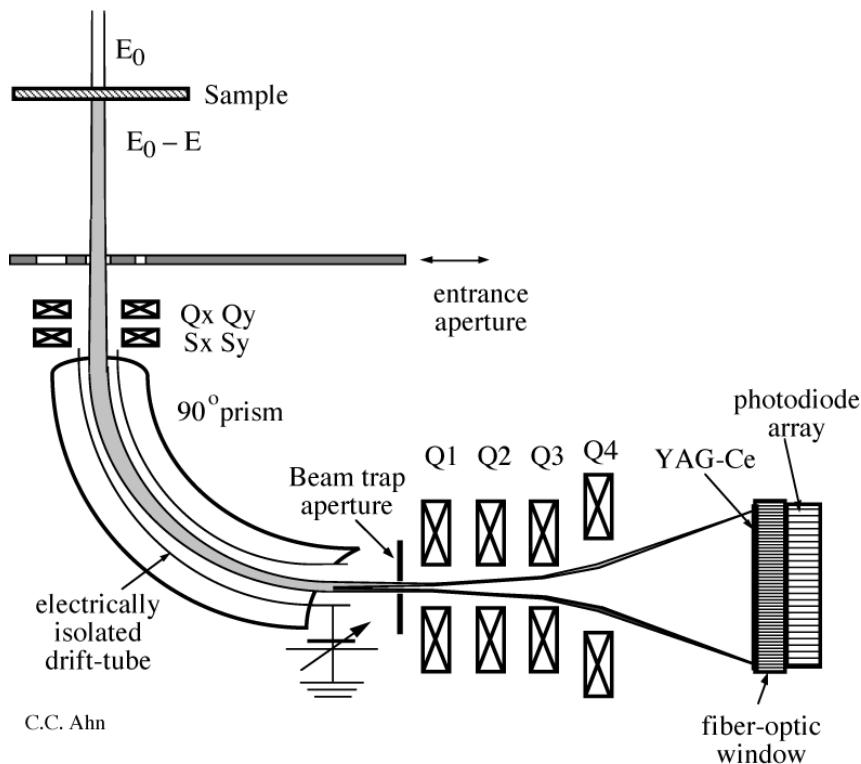
operation is especially useful for spectroscopy work, since it permits the acquisition of a “chemical map” of the sample. For example, we could make an image of the distribution of Fe in a sample if we were to measure, in synchronization with the raster pattern, either the emission of Fe $K\alpha$ x-rays (with the EDS spectrometer) or the numbers of transmitted electrons that undergo energy losses greater than that of the Fe L -edge (with the EELS spectrometer). An annular dark-field detector can also be used in the STEM mode of operation to for high-angle annular dark-field (or “ Z -contrast”) imaging. This HAADF method uses incoherent elastic scattering of electrons to form images of atom columns.

Besides the seven main techniques of:

- conventional imaging (bright-field and dark-field TEM),
- electron diffraction (selected area electron diffraction, SAD),
- convergent-beam electron diffraction (CBED),
- phase-contrast imaging (high-resolution TEM, HRTEM),
- Z -contrast imaging,
- energy-dispersive x-ray spectroscopy (EDS),
- electron energy-loss spectroscopy (EELS),

it is possible to perform many other experiments in a TEM.

4. Inelastic Electron Scattering and Spectroscopy



4.1 Inelastic Electron Scattering

Principles. This Chapter 4 first describes how high-energy electrons are scattered inelastically by materials, and then explains how electron energy-loss spectrometry (EELS) is used in materials research. Inelastic scattering occurs by the processes listed below in order of increasing energy loss, E . Energy is conserved in these inelastic processes – the spectrum of energy gains by the sample is mirrored in the spectrum of energy losses of the high-energy electrons.

Electrons undergoing energy losses to crystal vibrations, quantized as *phonons* with $E \sim 10^{-2}$ eV, are indistinguishable from elastically scattered electrons, given the present state-of-the-art for EELS in a TEM.

With modern instrumentation, it is possible to measure *interband transitions* of electrons from occupied valence bands to unoccupied conduction bands of semiconductors and insulators. With $E \sim 2$ eV, these spectral features are quite close in energy to the intense zero-loss peak from elastic scattering, so resolving them has been a challenge.

In many solids, especially metals, the bonding electrons can be understood as a gas of free electrons. When a high-energy electron suddenly passes through this electron gas, *plasmons* may be created. Plasmons are brief oscillations of the free electrons, giving broadened peaks in EELS spectra. Plasmon energies ($E \sim 10$ eV) increase with electron density, so plasmon spectra can be used to estimate free electron density. Plasmon spectra are also useful for measuring the thickness of a TEM specimen because more plasmons are excited as the electron traverses a thicker specimen.

Electrons that ionize atoms by causing *core excitations* are used for microchemical analysis. Chemical spectroscopy with EELS measures the intensities of “absorption edges,” which are jumps in spectral intensity at the threshold energies for ejecting core electrons from atoms in the material ($10^2 < E < 10^4$ eV). After a core electron has been excited from the atom, the remaining “core hole” decays quickly, often by the emission of a characteristic x-ray. Characteristic x-rays with energies from $>10^2$ to $>10^4$ eV are used in energy dispersive x-ray spectrometry (EDS) for chemical analysis.

Methods. “Analytical transmission electron microscopy” uses EDS or EELS to identify the elements in a specimen, and to measure elemental concentrations or spatial distributions. To quantify chemical concentrations, a background is subtracted to isolate the heights of absorption edges (EELS) or the intensities of peaks in an x-ray energy spectrum (EDS). These isolated intensities are then compared for the different elements in the specimen, and often converted into absolute concentrations with appropriate constants of proportionality. The accuracy of quantification depends on the reliability of these constants, so significant effort has been devoted to understanding them.

In this chapter, after brief descriptions of an EELS spectrometer and features of a typical EELS spectrum, plasmon energies are discussed with a simple model of a free electron gas. The section on “core excitations” provides a higher-level treatment of how a high-energy electron can cause a core electron to be ejected from the atom. It turns out that the probability of a core electron excitation is proportional to the square of the Fourier transform of the product of the initial and final wavefunctions of the excited electron. The cross-section for inelastic scattering also has an angular dependence that must be considered when making quantitative measurements with EELS. Some experimental aspects of EELS measurements are presented, including energy-filtered TEM imaging.

This chapter then presents the principles of EDS in the TEM, which involves more physical processes than EELS. Interestingly, the cross-section for core ionization decreases with atomic number, but the cross-section for x-

ray emission increases with atomic number in an approximately compensating way. This gives EDS spectrometry a balanced sensitivity for most elements except the very lightest ones.

4.2 Electron Energy-Loss Spectrometry (EELS)

4.2.1 Instrumentation

Spectrometer. After electrons have traversed a TEM specimen, a significant minority of them have lost energy to plasmons or core excitations, and exit the specimen with energies less than the energy of the incident electrons, E_0 (E_0 may be $200,000 \pm 0.5$ eV, for example). To measure the energy spectrum of these losses, an EELS spectrometer can be mounted after the projector lenses of a TEM. The heart of a transmission EELS spectrometer is a magnetic sector, which serves as a prism to disperse electrons by energy. In the homogeneous magnetic field of the sector, Lorentz forces bend electrons of equal energies into arcs of equal curvature. Some electron trajectories are shown in Fig. 4.1.

The spectrometer must allow an angular range for electrons entering the magnetic sector, both for reasons of intensity and for measuring how the choice of scattering angle, ϕ , affects the spectrum (cf., (4.44)). A well-designed magnetic sector provides good focusing action. Focusing in the plane of the paper (the equatorial plane) is provided by the magnetic sector of Fig. 4.1 because the path lengths of the outer trajectories are longer than the path lengths of the inner trajectories. It is less obvious, but also true, that the fringing fields at the entrance and exit boundaries of the sector provide an axial focusing action. With good electron optical design, the magnetic sector is “double-focusing” so that the equatorial and axial focus are at the same point on the right of Fig. 4.1. Since the energy losses are small in comparison to the incident energy of the electrons, the energy dispersion at the focal plane of typical magnetic sectors is only a few microns per eV.

Electrons that lose energy to the sample move more slowly through the magnetic sector, and are bent further upwards in Fig. 4.1.¹ In a “serial spectrometer,” a slit is placed at the focal plane of the magnetic sector, and a scintillation counter (see Sect. 1.4.1) is mounted after the slit. Intensity is recorded only from those electrons bent through the correct angle to pass through the slit. A range of energy losses is scanned by varying the magnetic field in the spectrometer. A “parallel spectrometer,” shown in the chapter title image, covers the focal plane of the magnetic sector with a scintillator and a position-sensitive photon detector such as a photodiode array. The post-field lenses Q1–Q4 magnify the energy dispersion before the electrons reach the scintillator. A parallel spectrometer has an enormous advantage over a

¹ Their longer time in the magnetic field overcomes the weaker Lorentz forces.

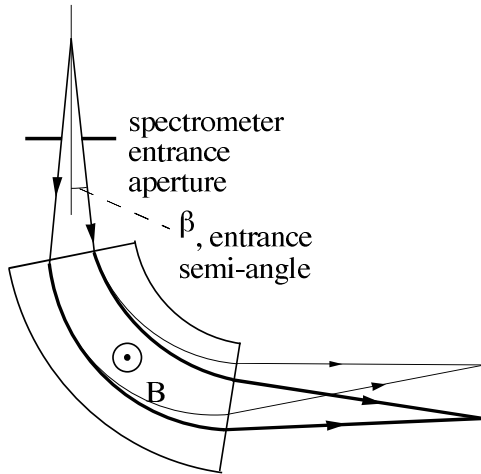


Fig. 4.1. Some electron trajectories through a magnetic sector with uniform magnetic field, B . The light curves are trajectories for lower-energy electrons (those with larger energy loss, E), and heavier curves are for higher-energy electrons. The collection semi-angle of the spectrometer is β .

serial spectrometer in its rate of data acquisition, but it requires calibrations for variations in pixel sensitivity.

The optical coupling of a magnetic sector spectrometer to the microscope usually puts the object plane of the spectrometer at the back focal plane of the final projector lens (Fig. 2.45). This back focal plane contains the diffraction pattern of the sample when the microscope is in image mode. When the microscope is operated in image mode, the spectrometer is therefore said to be “diffraction-coupled” to the microscope. With diffraction coupling, the collection angle, β , of the spectrometer is controlled by the objective aperture of the microscope. Alternatively, when the microscope is operated in diffraction mode, the back focal plane of the projector lens contains an image, and the spectrometer is said to be “image-coupled” to the microscope. With image-coupling, the collection angle, β , is controlled by an aperture at the entrance to the spectrometer (at top of Fig. 4.1).

Monochromator. The typical energy resolution for EELS spectrometers was about 1 eV or so for many years, but recent developments have allowed energy resolutions better than 0.1 eV on commercial microscopes. This is accomplished by starting with a field emission gun, often a Schottky effect gun (Sect. 2.4.1), followed by an electron monochromator, often a Wien filter as described here. Electrons traveling through a Wien filter encounter a region with crossed electric and magnetic fields that induce competing forces on the electron. In a Wien filter these electric and magnetic forces are tuned to cancel for electrons of one velocity, v_0 , which avoid deflection and pass through the exit aperture of the filter. Specifically, for an electron with velocity v_z down the optic axis along \hat{z} , a magnetic field oriented along \hat{y} produces a force along \hat{x} , $F_x^{mag} = ev_z B_y$. A Wien filter has an electric field along \hat{x} in the same region, generating a force on the electron of $F_x^{el} = -eE_x$. The special condition of cancelling forces, $F_x^{mag} = -F_x^{el}$, can be true for electrons of only one velocity, v_0 :

$$\begin{aligned}
ev_0B_y &= eE_x, \\
v_0 &= \frac{E_x}{B_y}.
\end{aligned}
\tag{4.1}$$

Electrons with velocities differing from v_0 are deflected, and do not pass through the exit aperture of the Wien filter. In practice, it is typical to operate the Wien filter at a voltage close to that of the electron gun itself, so the electron velocity through the filter will be slow enough that sub-eV resolution is possible with reasonable values of electric field, magnetic field, and aperture size. Biasing the Wien filter assembly near -100 or -200 keV can be challenging, however.

The Wien filter first disperses electrons of different energies into different angles, and then allows electrons of only a selected energy to pass through its exit aperture. Monochromatization therefore discards a substantial fraction of electrons – perhaps 80% of the electrons are lost when monochromating to 0.1 eV. When operating in STEM mode, the electron current is also reduced substantially when forming the smallest electron probes. It is typical to make compromises between the brightness of the image, the electron monochromatization, and the size of the probe – an increase in one usually requires a decrease in another. Manufacturers are constantly trying to find ways to improve these aspects of microscope performance.

4.2.2 General Features of EELS Spectra

A typical EELS spectrum is presented in Fig. 4.2. The enormous “zero-loss peak” is from electrons of 200,000 eV that passed through the specimen without any energy loss. The sharpness of this peak indicates that the energy resolution is about 1.5 eV. The next feature is at the energy loss $E = 25$ eV, from electrons having energies of 199,975 eV. It is the “first plasmon peak,” caused by the excitation of one plasmon in the sample. With thicker specimens there may also be peaks at multiples of 25 eV from electrons that excited two or more plasmons in the specimen. The small bump in the data at 68 eV is not a plasmon peak, but rather a core loss. Specifically it is a Ni $M_{2,3}$ absorption edge caused by the excitation of $3p$ electrons out of Ni atoms. An enormous feature is seen at an energy loss of about 375 eV, but it is an artifact of the serial data acquisition method, and not a feature of the material. (At 375 eV the detector operation was changed from measuring an analog current to the counting of individual electron events.)

The background in the EELS spectrum falls rapidly with energy (the denominator of Δk^2 in (4.28) is partially responsible for this), and the next feature in the Ni spectrum of Fig. 4.2 is a core loss edge at 855 eV. This feature is caused by the excitation of $2p^{3/2}$ electrons out of the Ni atom, and is called the “ L_3 edge.” The L_2 edge at 872 eV is caused by the excitation of $2p^{1/2}$ electrons out of the atom. Right at the L_2 and L_3 edges are sharp, intense peaks known as “white lines” that originate from the excitation of $2p$

4.3 Plasmon Excitations

4.3.1 Plasmon Principles

A fast electron jolts the free electrons when it passes through a material. This displaced charge creates an electric field to restore the equilibrium distribution of electrons, but the charge distribution oscillates about equilibrium for a number of cycles. These charge oscillations are called “plasmons,” and are quantized in energy. Larger energy losses correspond to the excitation of more plasmons, not to an increase in the energy of a plasmon. In most EELS spectra, the majority of inelastic scattering events are plasmon excitations.

To find the characteristic oscillation frequency of a plasmon, consider the rigid translation of a wide slab of electron density by a small amount, x , as in Fig. 4.7. At the bottom surface of the slab all the electrons are removed, but at the top the electron density is doubled. This charge disturbance therefore sets up the electric field, \mathcal{E} , of a parallel-plate capacitor:

$$\mathcal{E} = 4\pi\sigma_s , \tag{4.4}$$

where σ_s is the surface charge density equal to the electron charge, e , times ρ , the number of electrons per unit volume, times the displacement, x :

$$\sigma_s = e\rho x . \tag{4.5}$$

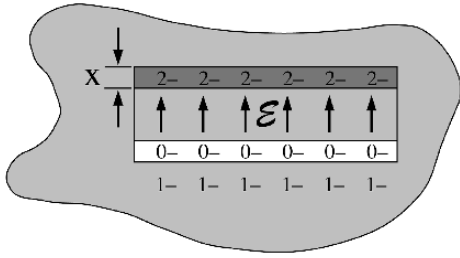


Fig. 4.7. Displacement of a slab of electric charge, leading to doubling of the charge density at the top of the slab over thickness x , and depletion of charge at the bottom. A wide, flat slab idealizes the problem as one dimensional.

The field, \mathcal{E} , provides the restoring force to move the electron slab back to its original position. The electrostatic restoring force *per unit volume* of slab is:

$$F = -e\rho\mathcal{E}. \quad (4.6)$$

Substituting (4.5) into (4.4), and then into (4.6) provides:

$$F = -e^2\rho^2 4\pi x. \quad (4.7)$$

The Newtonian equation of motion per unit volume of the electron slab is:

$$F = \rho m_e \frac{d^2x}{dt^2}. \quad (4.8)$$

Substituting (4.7) into (4.8) gives:

$$\frac{d^2x}{dt^2} = -\left(\frac{4\pi e^2\rho}{m_e}\right)x. \quad (4.9)$$

Equation (4.9) is the equation of motion for an undamped harmonic oscillator with the characteristic frequency:

$$\omega_p = \sqrt{\frac{4\pi e^2\rho}{m_e}} = 5.64 \times 10^4 \sqrt{\rho}, \quad (4.10)$$

where the units of ρ are [electrons cm^{-3}], and ω_p is [Hz]. With analogy to a mechanical oscillator, the electron density provides the stiffness. The higher the electron density, the higher the plasmon frequency. For metals, assuming an approximate free electron density of $\rho = 10^{23}$ electrons cm^{-3} , $\omega_p \simeq 2 \times 10^{16}$ Hz.³ The characteristic energy of such an oscillation is the plasmon energy, given by:

$$E_p = \hbar\omega_p, \quad (4.11)$$

and for our example $E_p = (6.6 \times 10^{-16} \text{ eV s})(2 \times 10^{16} \text{ s}^{-1}) \approx 13 \text{ eV}$.

In EELS, intense plasmon peaks are prominent at energy losses of 10–20 eV. Plasmons are not long-lived, however, often because they promote

³ The present one-dimensional approach is not necessarily reliable for relating the free electron density to the plasmon energy. A more general approach uses the imaginary component of the dielectric constant of the material, and the theory uses the mathematics discussed in Problem 4.6.

excitations of electrons near the Fermi energy. Plasmon peaks therefore tend to be broadened in energy.⁴ Free electron metals such as aluminum have sharper plasmon peaks than do alloys of transition metals, which have a high density of states at the Fermi energy. Compared to core electron excitations, however, plasmon excitations do not provide much detailed information about the individual atom species in the material.

4.3.2 * Plasmons and Specimen Thickness

The characteristic length or “mean free path,” $\bar{\lambda}$, over which a 100 keV electron excites one plasmon is about 100 nm in metals and semiconductors. This is an average length, so in a TEM specimen of even 50 nm, some electrons excite one, two, or more plasmons. The probability P_n for the excitation of n plasmons in a sample of thickness, t , is determined by the statistics of Poisson processes:

$$P_n = \frac{1}{n!} \left(\frac{t}{\bar{\lambda}} \right)^n e^{-t/\bar{\lambda}} = \frac{I_n}{I_t}, \quad (4.12)$$

where I_n is the number of counts in the n^{th} plasmon peak, and I_t is the number of counts in all plasmon peaks with $n \geq 0$ (I_t includes the zero-loss peak for which $n = 0$). The EELS spectrum in Fig. 4.8 shows distinct plasmon peaks. After subtracting a background from other inelastic processes (originating with the Al L -edge and a contribution from oxides and the substrate), P_n is obtained as the fractional area of the n^{th} plasmon peak.

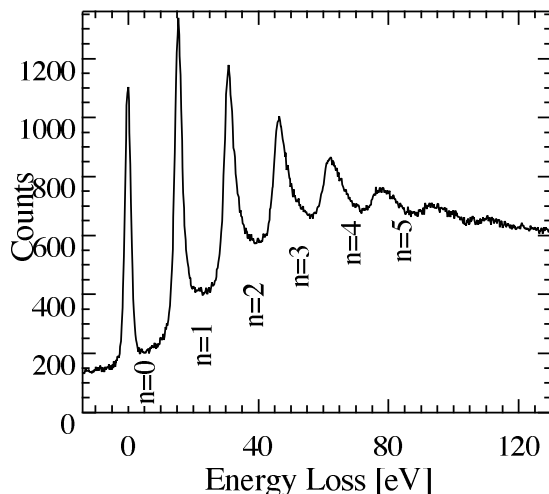


Fig. 4.8. Low-loss spectrum taken from a thick sample of ~ 120 nm Al metal on C using 120 keV electrons and $\beta = 100$ mrad. Plasmon peaks are visible at energies of $n \times 15$ eV, where n is the number of plasmons excited in the sample. After [4.4].

Good samples for TEM imaging are several times thinner than the sample used for Fig. 4.8, but plasmon peak areas still offer a practical way to

⁴ “Lifetime broadening” is understandable from the uncertainty principle: $\Delta E \Delta t \simeq \hbar$. A short lifetime Δt comes with a large uncertainty in energy, ΔE .

determine thicknesses of thin samples. Setting $n = 0$ in (4.12), the thickness, t , is:

$$\frac{t}{\bar{\lambda}} = \ln\left(\frac{I_t}{I_0}\right). \quad (4.13)$$

Measurement of I_t and I_0 (the zero-loss or the $n = 0$ plasmon peak) involves the choice of the energies ε , δ and Δ , which define the limits of integration, as illustrated in Fig. 4.9.⁵ The lower limit ($-\varepsilon$) of the zero-loss region can be taken anywhere to the left of the zero-loss peak where the intensity has decreased to zero, the separation point δ between the zero-loss and inelastic regions may be taken as the first minimum in intensity, and $\Delta \approx 100$ eV is usually sufficient to include most of the inelastic scattering in relatively thin, low Z materials (for high Z and/or thick specimens, several hundred eV should be used since the scattered intensity is shifted to higher energy loss). Equation (4.13) has been shown to give 10% accuracy for relative thickness measurements on samples as thick as $t = 5\bar{\lambda}$. Some deviations from the intensities of (4.12) are of course expected when the electron beam passes through regions of non-uniform thicknesses or composition, and when other contributions are present in the low-loss spectrum.

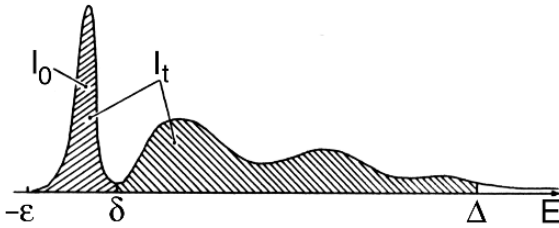


Fig. 4.9. The integrals and energies involved in measuring specimen thickness by the log-ratio method. After [4.5].

Absolute determinations of specimen thickness require values for the total inelastic mean free path. For materials of known composition, it is possible to calculate a value for the mean free path according to the semi-empirical equation [4.5]:

$$\bar{\lambda} \approx \frac{106 F}{\ln(2\beta E_0/E_m)} \frac{E_0}{E_m}, \quad (4.14)$$

where units for $\bar{\lambda}$ are [nm], β is the collection semiangle [mrad], E_0 is the incident energy [keV], E_m is a mean energy loss [eV] that depends on the composition of the sample, and F is a relativistic factor:

$$F = \frac{1 + E_0/1022}{(1 + E_0/511)^2}, \quad (4.15)$$

⁵ If a collection aperture limits the angles recorded by the spectrometer to a maximum angle β , $\bar{\lambda}$ in (4.13) must be interpreted as an effective mean free path, $\bar{\lambda}(\beta)$.

and $F = 0.768$ for $E_0 = 100$ keV and 0.618 for $E_0 = 200$ keV. For a specimen of average atomic number Z , E_m can be obtained from the semi-empirical formula:

$$E_m \approx 7.6Z^{0.36} . \quad (4.16)$$

For large collection apertures, i.e., $\beta > 20$ mrad for $E_0 = 100$ keV or $\beta > 10$ mrad at 200 keV, (4.14) becomes inapplicable and the mean free path saturates at a value independent of β .

Specimen thickness measurement by this EELS plasmon technique has some advantages over other techniques for measuring specimen thickness (such as CBED) because it can be applied for a wide range of specimen thicknesses, including very thin specimens, and for specimens that are highly disordered or amorphous. Table 4.1 lists some values for calculated (with (4.10) and (4.11)) and measured plasmon energies E_p , widths of the plasmon peaks ΔE_p , characteristic scattering angles for plasmons ϕ_{E_p} , and calculated mean free paths $\bar{\lambda}$, for 100 keV incident electrons.

Table 4.1. Plasmon data for selected materials [4.5]

Material	E_p (calc.) (eV)	E_p (expt.) (eV)	ΔE_p (eV)	ϕ_{E_p} (mrad)	$\bar{\lambda}$ (nm)
Li	8.0	7.1	2.3	0.039	233
Be	18.4	18.7	4.8	0.102	102
Al	15.8	15.0	0.5	0.082	119
Si	16.6	16.5	3.7	0.090	115

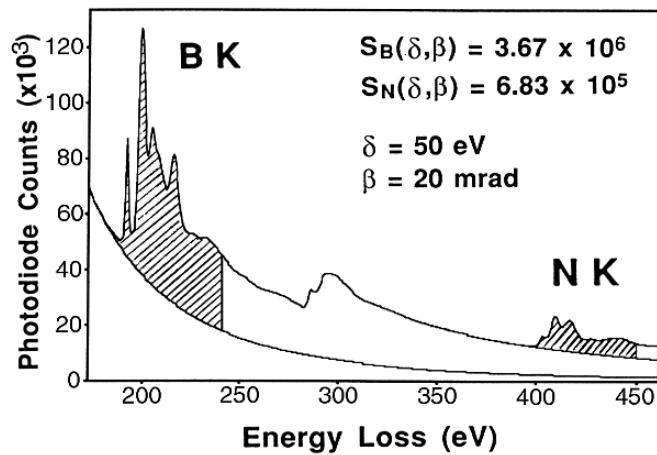


Fig. 4.15. Chemical composition determination of BN. Background fits are shown, as are the 50 eV ranges of energy integration, δ . Using a collection aperture angle of 20 mrad, the partial ionization cross-sections were calculated with (4.52). Agreement was within 4% of the known composition of B–50 at.% N. After [4.7].

4.5 Energy-Filtered TEM Imaging (EFTEM)

4.5.1 Spectrum Imaging

Chemical mapping of the element distributions in samples is possible when EELS is performed in STEM mode (Fig. 2.1). The electron beam is focused into a small probe and EELS spectra are acquired from a two-dimensional grid of points across the sample. Each “pixel” in the image can contain an entire EELS spectrum. The data set, called a “spectrum image,” contains a wealth of information on chemical variations across the specimen. Analysis of this chemical information follows procedures of EELS spectrometry described in Sects. 4.2–4.4. Unfortunately, it may take hours to acquire a complete spectrum image. Exposing a sample to a high-intensity probe beam for a long time often causes problems with contamination and radiation damage. Over long times the specimen may also drift in position, blurring the image.

4.5.2 Energy Filters

Another method for chemical mapping has become popular, but it requires specialized instrumentation. Because an EELS spectrum consists of electrons that pass through the specimen and through the optical system of the TEM, the optical system can be used to make images of inelastically-scattered electrons. A conventional TEM uses all electrons that pass through the sample, but an instrument or an instrument modification known as an “energy filter” allows image formation with electrons that have undergone selected energy losses in the specimen. The technique of “energy-filtered TEM” (EFTEM), detects “chemical contrast” in specimens by adjusting an energy filter to pass

electrons that have lost energy to core ionizations of selected elements.¹⁵ Under optimal conditions, these “energy-filtered images” (EFI) can reveal chemical contrast with sub-nanometer spatial resolution.

Alternatively, an energy filter can pass only zero-loss electrons, thereby removing all inelastic scattering from a conventional image or diffraction pattern. By using pure elastically-scattered electrons, chromatic aberration and the inelastic background are eliminated, so improved contrast is possible for thicker specimens, and more reliable interpretations of both images and diffraction patterns are possible. Energy filters will probably find a wider use for chemical analysis at the near-atomic scale, however, so this is the focus of the present discussion.

Figure 4.16a shows a modification of the magnetic prism EELS spectrometer shown previously in Fig. 4.1. As mentioned in Sect. 4.2.1, the magnetic sector operates as a focusing lens, and its optical analog is shown in Fig. 4.16b. By comparing the ray paths in Figs. 4.16a and b, it is evident that the magnetic sector effectively bends the ray diagrams of Fig. 4.16b. As in Fig. 4.1, the thin rays in Fig. 4.16a correspond to trajectories of electrons that have experienced energy losses, and the thick rays correspond to the zero-loss electrons. Notice how the thin and thick rays have the same pattern, but the thin rays are bent by an additional angle. The aperture at the image plane in Fig. 4.16a has been positioned to remove the zero-loss electrons. Additional lenses to the right of the energy-selecting slit in Fig. 4.16a (such as Q1–Q4 in the title image of Chapter 4) are used to project the energy-filtered image (EFI) onto an area detector such as a scintillator with a CCD camera.

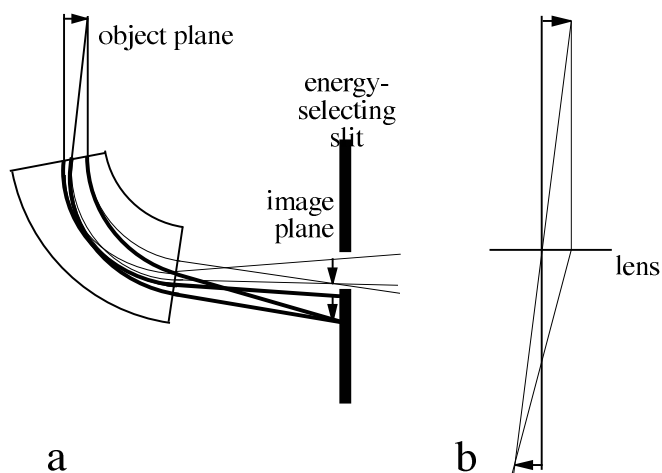


Fig. 4.16. (a) An energy filter based on a magnetic sector like that in Fig. 4.1. (b) Optical analogy for monochromatic electrons.

Chapter 2 described how lenses produce dispersions of positional information (images) and angular information (diffraction patterns). The energy filter of Fig. 4.16 also produces a dispersion of electron energies (an EELS spectrum). This particular energy filter focuses an arrow on the object plane

¹⁵ Plasmon images may also be useful.

(a diffraction pattern or an image at the back focal plane of the final projector lens) onto an arrow at the image plane. In this case the image plane happens to be the same plane as the energy dispersion plane (as in Fig. 4.1). Selecting a narrow range of energy therefore limits the field of view of the image, so at the energy-selecting slit it may be appropriate to form a small image with a low magnification (or a small diffraction pattern) and magnify it with subsequent lenses.

Ensuring a good resolution of Δk , good spatial resolution, and high energy selectivity is a challenge for an energy filter, because it must also allow for measurements over wide ranges of these variables Δk , x , and E . Its performance is degraded by various types of aberrations. Recall (Sect. 2.7.1) that spherical aberration mixed angular and spatial information – spherical aberration caused errors in position (x) at the focal plane for rays leaving the specimen at different angles (Δk). An energy filter has aberrations that mix energy, angular, and spatial information. For example, not all locations on an EFI may correspond to the same energy loss. In analogy to the apertures used to suppress problems with spherical aberration, energy filters require apertures to limit their field of view, their angular acceptance, or their acceptance window of energy losses.

To optimize imaging performance, it is best for electrons of only one energy to pass through the objective lens. Energy filters are integrated into the microscope electronics to achieve this by allowing the energy filter system to control the high voltage at the electron gun. For making images with electrons that have undergone an energy loss of $e\Delta V$, the high voltage is increased by the amount ΔV . With such control over the high voltage system, the focus can then be adjusted only once, and focus will be maintained for images of electrons that have undergone different losses in the sample. The change in incident energy of the electrons then requires that the condenser lens currents are also tuned by the electronics of the energy filter system. This ensures a consistent intensity of illumination on the specimen, important for quantitative work.

Chemical analysis by EFTEM usually identifies elements by their core-loss spectra. For the thin specimens needed for EFTEM, however, only a small fraction of the incident electrons can ionize atoms in the sample. A central concern, therefore, is collecting as many inelastically-scattered electrons in as short a time as possible to minimize the effects of specimen drift, contamination, or radiation damage. This motivates the use of large apertures and wide energy windows, pushing the limits of filter performance. For example, more intensity is possible with a wider energy window, but a wider range of energies increases the effects of chromatic aberration, leading to a loss of spatial resolution. Fortunately, in spite of these challenges, many types of chemical analyses with sub-nanometer resolution are now possible with EFTEM.

4.5.3 Chemical Mapping with Energy-Filtered Images

The ability to quantify chemical information at a near-atomic scale (including light elements such as C, O and N) makes EFTEM an important tool for materials characterization. Chemical information is usually obtained from the increase (or “jump”) in EELS spectral intensity at an absorption edge. Unfortunately, absorption edges reside on a large, sloping backgrounds from plasmons or absorption edges of other elements. Chemical mapmaking therefore requires EFIs at energy losses both above and below an absorption edge. Data processing is then needed to isolate the chemical information from the background. For example, the chemical contrast in an image acquired above the absorption edge, the “post-edge” image, can be better seen by subtracting or dividing by an image of the background obtained from “pre-edge” EFIs.¹⁶ Two types of elemental maps are typically used:

- a “jump-ratio image,” where a post-edge image is divided by a pre-edge background image,
- a “three-window image,” where intensities in two pre-edge images are extrapolated to the energy of the post-edge image, and subtracted from it.

Jump-ratio images have the advantage that variations in specimen thickness and diffraction contrast are largely cancelled by the division. The three-window image provides better elemental quantification, however. Unfortunately, three-window images are generally noisier than jump-ratio images owing to the background subtraction procedure, and may require longer times for measurement.

A first step in obtaining a chemical map with EFTEM is acquiring an EELS spectrum to locate the edges of interest, decide on placement of the energy windows, and determine the suitability of the specimen thickness. Another preparatory step is tilting the sample or incident beam to minimize the diffraction contrast in the bright-field TEM image. Since elastic scattering can be much stronger than inelastic scattering, diffraction contrast can dominate the appearance of energy-filtered images. To increase the relative amount of chemical contrast, the sample should be tilted away from strong diffraction conditions. Six EFIs of the same region are useful for making chemical maps. These images (with approximate energy windows) are:

- Unfiltered (bright field) image (all energies),
- Zero-loss image (5–10 eV),
- Low-loss (plasmon) image (20 eV),
- Pre-edge image 1 (10–20 eV),
- Pre-edge image 2 (10–20 eV),
- Post-edge image (10–20 eV).

¹⁶ For example, the counts in each pixel of a background image could be subtracted from the counts in each corresponding pixel of the post-edge EFI.

For thin samples, the intensity of the inelastic spectrum is proportional to the sample thickness. Variations in sample thickness do not distort ratios of element concentrations if they are obtained as ratios of images from different elemental edges. When examining the chemical map of one element, however, it is important to know how the thickness varies across the sample. Since the unfiltered image contains both the elastically- and inelastically-scattered electrons, while the zero-loss image contains only elastically-scattered electrons, it is possible to divide the unfiltered image by the zero-loss image and take the logarithm of the result to obtain a thickness map in units of t/λ (as described in Sect. 4.3.2). This thickness map can be used to identify irregular sample surfaces, and permits conversion from areal densities of atoms to absolute concentrations. Similarly, three-window images can be corrected for the effects of thickness by dividing by the low-loss image.

For EFIs, the best specimen and microscope parameters are usually similar to those for EELS. For example, as in EELS, the specimen should be very thin, i.e., $t/\lambda < 0.5$, and ideally about half this thickness.¹⁷ A rule-of-thumb is that the plasmon peak should be no more than one-fifth the height of the zero-loss peak. Similarly, a small collection angle (5-10 mrad) is preferable because it usually increases the signal/background ratio of an edge (see Problem 4.9). Elements of atomic number greater than 12 allow a choice of edge energy for elemental analysis. It is best to use major edges, and those with threshold energies from 100 to 1000 eV. At lower energies diffraction contrast and a steep background complicate quantification. Spatial resolution is also impaired for energy losses below 50 eV because ionization becomes delocalized, not necessarily occurring at the atoms nearest the high-energy electron. At energies above 1000 eV the intensity becomes inconveniently low. This often requires a wider window for energy selection, leading to problems with chromatic aberration. Effects of chromatic aberration can be suppressed by using smaller objective apertures, but this restricts the range of Δk , and hence the spatial resolution (cf. (2.11)).

4.5.4 Chemical Analysis with High Spatial Resolution

Figures 4.17 and 4.18 illustrate several aspects of making chemical maps by EFTEM imaging. The experiment confirmed that Ag enrichment was responsible for the conventional contrast of two planes at the interface between an Ω -phase precipitate and an Al-rich matrix. The flatness of this internal interface was helpful for detecting chemical contrast at high spatial resolution.

The Ag $M_{4,5}$ edge has a delayed maximum, peaking about 50 eV above the edge onset (Fig. 4.17). For best intensity, the post-edge window should incorporate the intensity maximum of the absorption edge, but this required the pre-edge 2 image and the post-edge image to be recorded with a fairly

¹⁷ Deconvolution of plural scattering is not possible in EFTEM because a full spectrum is not acquired.

large energy separation. This is not optimal for EFTEM imaging. Better detectability and spatial resolution can be achieved when the windows labeled “pre-edge 2” and “post-edge” abut together at the onset of an abrupt absorption edge. Abrupt K -edges or intense, sharp white lines at the L -edges of transition metals offer this possibility. Additionally, spatial resolution can be improved by using energy windows narrower than the 30 eV windows used in this example, provided sufficient signal is available. Nevertheless, the research problem involved Ag, so the windows for the energy filter were chosen as in Fig. 4.17.

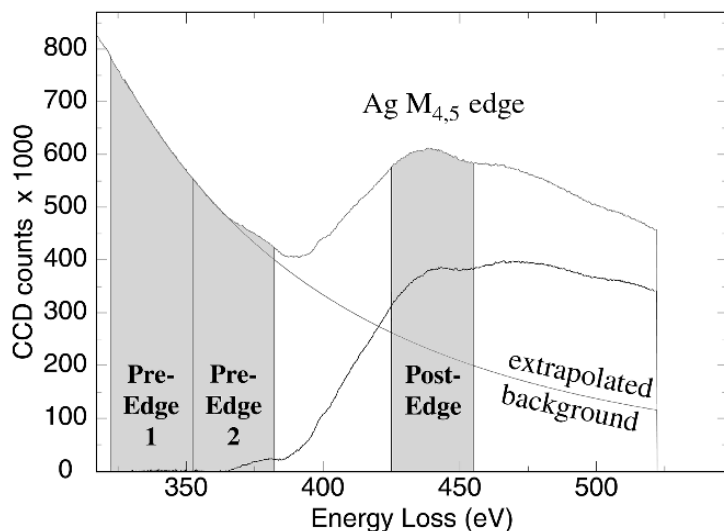


Fig. 4.17. A portion of an EELS spectrum showing the Ag $M_{4,5}$ edge and the placement of the pre-edge 1, pre-edge 2, and post-edge energy windows used for the EFIs in Fig. 4.18. An extrapolated background and a background-stripped Ag $M_{4,5}$ edge are also shown. After [4.8].

Figure 4.18 shows a set of EFTEM images of an Ω precipitate plate in an Al-Cu-Mg-Ag alloy. To suppress diffraction contrast, the sample was tilted off the exact $[011]$ zone-axis of the α -phase matrix, but the $\alpha|\Omega$ interfaces were still parallel to the electron beam. Two dark lattice-fringes can be seen at the $\alpha|\Omega$ interfaces on both sides of the Ω plate in the zero-loss image (Figs. 4.18a,b). These fringes are the width of two $\{111\}$ Al planes (0.46 nm). At each interface, both the Ag jump-ratio image and three-window image show high-intensity lines. The three-window image is noisier than the jump-ratio image, but provides a better estimate of the high enrichment of Ag. The background is featureless in both images, indicating that diffraction contrast and thickness effects are negligible. Two line profiles, acquired from the boxes shown in each image, are shown below the jump-ratio and three-window images. Both reveal segregation of Ag to the precipitate. These Ag layers are only 0.46 nm wide, showing the outstanding spatial resolution of the technique.

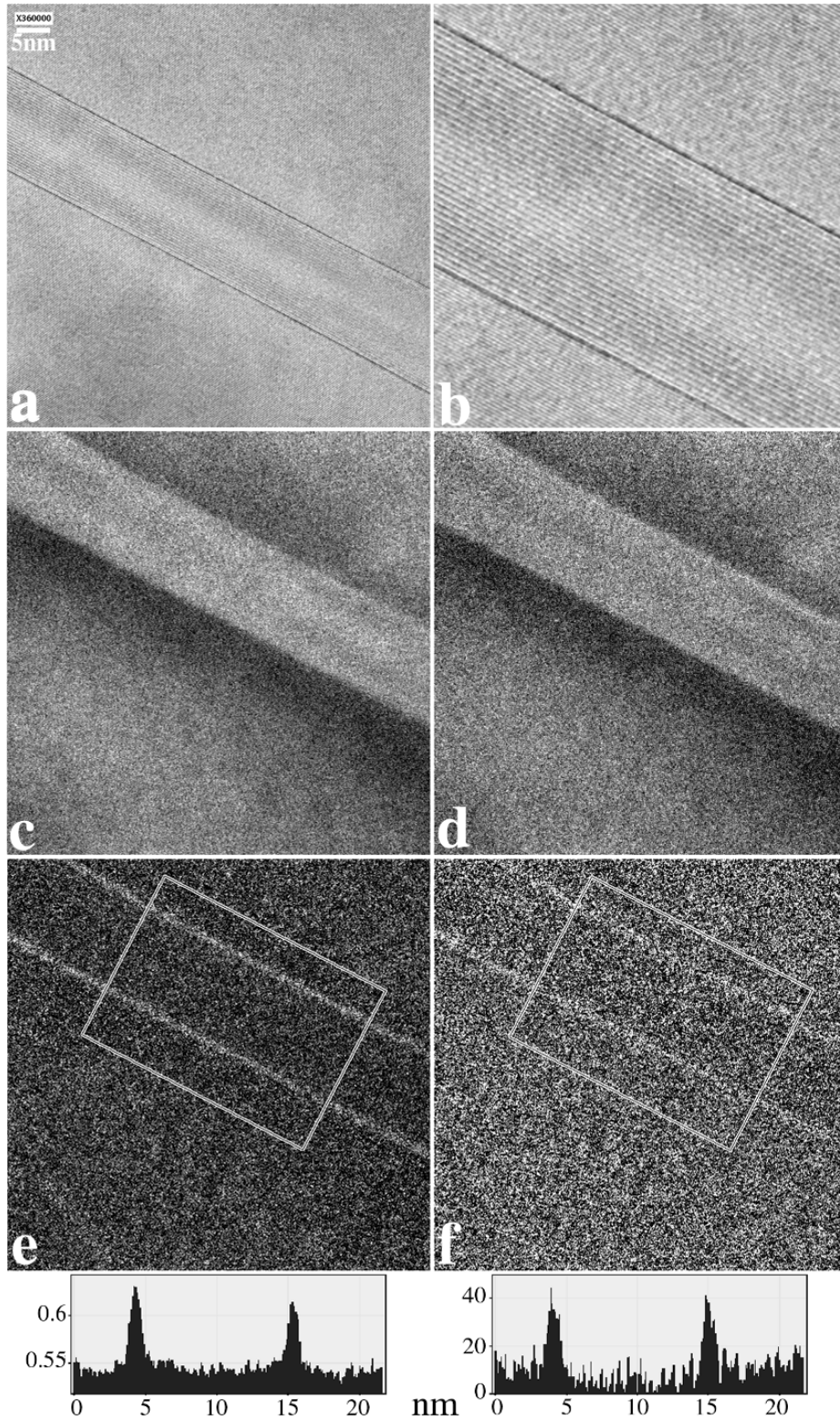


Fig. 4.18. A set of EFTEMs from an edge-on Ω -phase plate-shaped precipitate in an Al-Cu-Ag-Mg alloy (α -phase), acquired with the sample tilted so the habit-plane interfaces were parallel to the electron beam, but the sample was not directly on the zone axis. Some energy windows are shown in Fig. 4.17. (a) zero-loss image, (b) enlargement of part a, (c) pre-edge 2 image, (d) post-edge image, (e) Ag $M_{4,5}$ jump-ratio image, and (f) Ag $M_{4,5}$ three-window chemical map. Line profiles corresponding to e and f should be aligned along the short edge of the boxes enclosing the $\alpha|\Omega$ interfaces. ($\beta = 18$ mrad). After [4.8].